Science Advances

AAAS

advances.sciencemag.org/cgi/content/full/3/10/e1700909/DC1

Supplementary Materials for

Surface plasmon polariton laser based on a metallic trench Fabry-Perot resonator

Wenqi Zhu, Ting Xu, Haozhu Wang, Cheng Zhang, Parag B. Deotare, Amit Agrawal, Henri J. Lezec

Published 6 October 2017, *Sci. Adv.* **3**, e1700909 (2017)
DOI: 10.1126/sciadv.1700909

This PDF file includes:

- fig. S11. Grating optimization of the SPP-pumped SPP laser.
- fig. S12. Simulated steady-state intensity profiles for grating-decorated and grating-free Ag surfaces coated with a 260-nm-thick four-level gain medium.
- References (*36*, *37*)

section S1. Minimizing SPP propagation losses

To minimize absorption-induced SPP propagation loss in the red, the cavity is fabricated using Ag for the metal surfaces of the cavity. The propagation loss is further minimized by use of ultra-smooth template-stripped Ag, which have been shown to exhibit absorption-induced SPP propagation losses that are smaller than those of as-deposited Ag surfaces (*25*). The evaporated template-stripped Ag surfaces used in this study exhibit typical root-mean-square roughness of ≈ 2.9 nm as measured by an atomic force microscope (fig. S1).

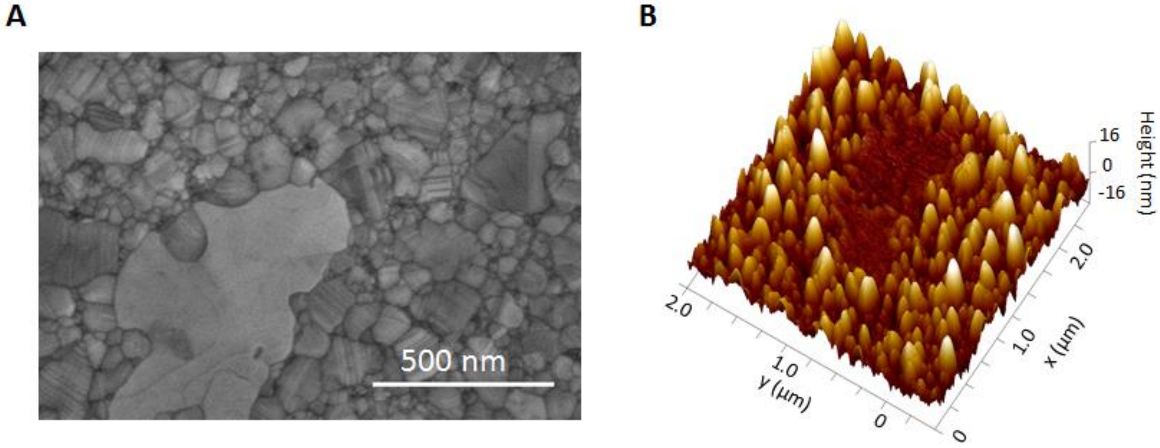

fig. S1. Surface morphology characterization of a template-stripped Ag film. (**A**) Top-down scanning electron microscope (SEM) image and (**B**) atomic force microscope (AFM) image of a template-stripped Ag-air interface. AFM measurements yield a root-mean-squared roughness of ≈ 2.9 nm and an arithmetic-average roughness of ≈ 2.1 nm.

The corresponding SPP propagation decay length L_x is experimentally measured (using the method described in ref. *25*) to be ≈ 25 μm at λ_0 = 650 nm (fig. S2, blue spheres), a value that closely matches the theoretical SPP decay length calculated using the bulk effective permittivity of template-stripped Ag measured by a spectroscopic ellipsometer (fig. S2, dashed black line).

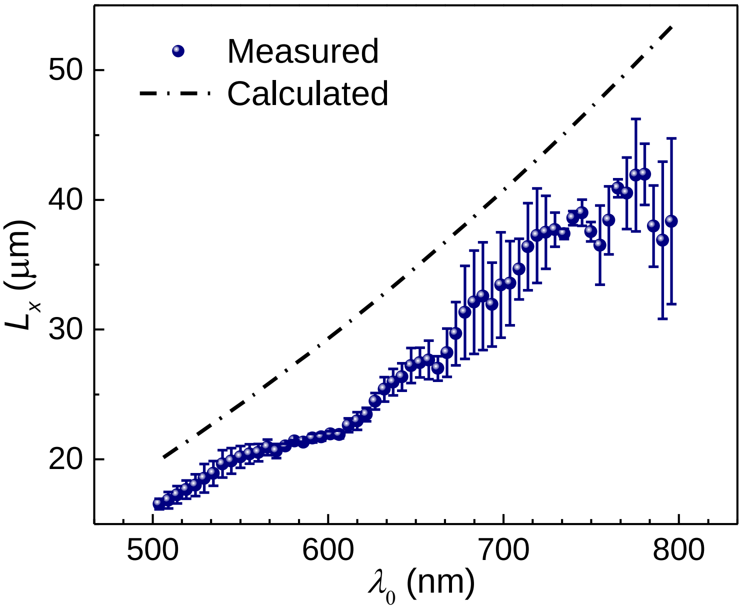

fig. S2. Propagation decay length of SPPs propagating on a template-stripped Ag-air interface. Experimentally measured 1/*e* decay length L_x of SPPs for free-space wavelengths ranging from 500 nm to 800 nm (blue spheres). The theoretical SPP decay length calculated using the bulk effective permittivity of template-stripped Ag (dashed black line).

section S2. Minimizing SPP reflection losses

Performing finite-difference time-domain (FDTD) simulations over the visible frequency range, the reflectance R_∞ of an SPP mode impinging on an infinitely tall, perfectly flat Ag mirror is analyzed as a function of angular deviation $\Delta\theta$ of the mirror with respect to the normal to the propagation-plane (fig. S3A). The SPP reflectance at $\lambda_0 = 650$ nm is maximum at normal incidence ($\Delta\theta = 0°$), yielding $R_\infty = 0.95$, and remains virtually constant (within the range $0.93 \leq R_\infty \leq 0.95$) for $|\Delta\theta| \leq 1°$, an angular deviation tolerance found to be feasible with fabrication sequence used in this study. The natural evanescent confinement of SPPs normal to the direction of propagation furthermore suggests the possibility of reducing the sidewall mirror heights to finite values such that scattering loss at the top of the sidewall remains minimal. FDTD simulations at $\lambda_0 = 650$ nm, assuming perfectly vertical sidewalls, are used to study the fundamental dependence of sidewall reflectivity R on sidewall height h.

FDTD simulations at $\lambda_0 = 650$ nm, assuming perfectly vertical sidewalls ($\Delta\theta = 0°$), are used to study the dependence of sidewall SPP reflectivity R on sidewall height h. Simulations show that R reaches values within 1 % of its asymptotic limit $R_\infty \approx 0.95$, for sidewall heights $h > 1.5$ µm (fig. S3B), in other words for heights exceeding by a factor of ≈ 4 the corresponding SPP decay length given by simulation ($d \approx 400$ nm).

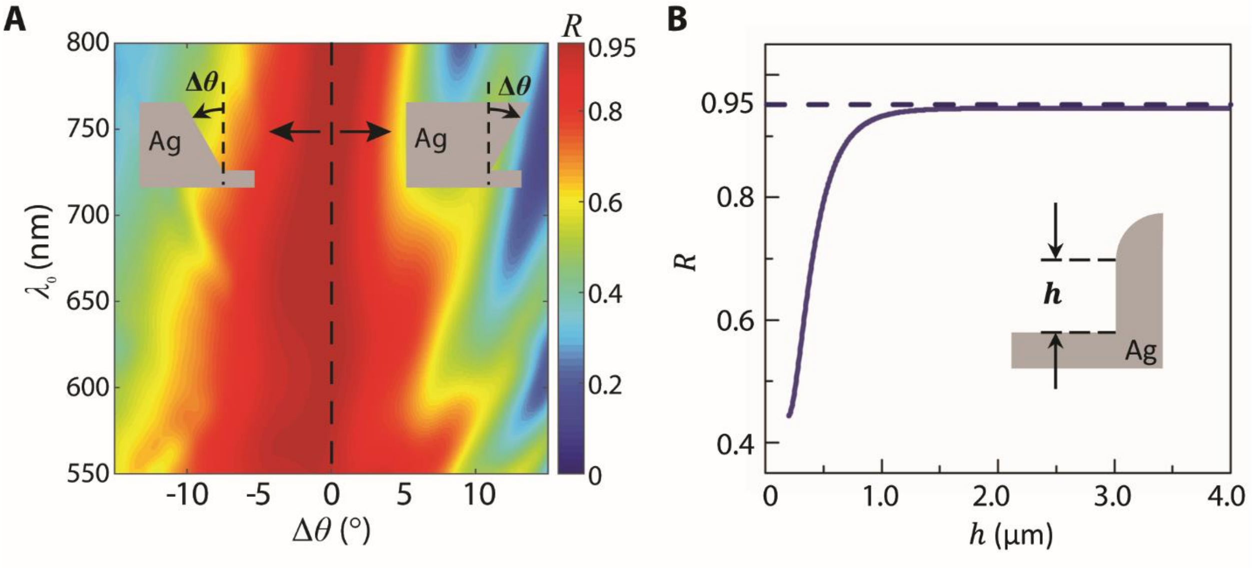

fig. S3. Optimization of SPP reflection losses. (**A**) FDTD simulations of reflectance R of an SPP mode impinging on an infinitely tall, perfectly flat Ag sidewall vs. angular deviation of sidewall from the surface normal, $\Delta\theta$ and free-space wavelength, λ_0. (**B**) Sidewall SPP reflectance R as a function of sidewall height h. The dashed blue line shows the SPP reflectance for an infinitely tall, perfectly flat and vertical Ag sidewall, $R_\infty \approx 0.95$. R asymptotically increases towards R_∞ as a function of increasing h, reaching values within 1 % of R_∞ for $h > 1.5$ µm.

section S3. Optimization of the length of the SPP Fabry-Perot cavity

Given a specific round-trip SPP loss, the length of the SPP Fabry Perot cavity governs the tradeoff between the highest achievable quality factor Q and Finesse $\mathcal{F}$ of a given resonance mode. The quality factor Q and Finesse $\mathcal{F}$ of a slit-free SPP Fabry-Perot cavity of length l, with an anticipated resonance frequency ν_0 (or free-space wavelength λ_0), can be estimated by using the lossy Fabry-Perot cavity model (*36*). Consistent with a free-space Fabry-Perot resonator, the resonance condition for a resonator utilizing SPPs propagating along a metal cavity floor enclosed by a pair of reflective sidewalls is reached when the cavity can trap an integer numbers of SPP half wavelengths, i.e. for cavity lengths

$$l = m\frac{\lambda_{\mathrm{SPP}}}{2}$$

where m is a positive integer $(1, 2, \ldots)$, and λ_{SPP} is the SPP wavelength (fig. S4A). At a free-space wavelength λ_0, the wavelength of an SPP mode propagating along a Ag-air interface is given by $\lambda_{\mathrm{SPP}} \approx \lambda_0/n_{SPP}$, where

$$n_{\mathrm{SPP}} = \mathrm{Re}\left[\sqrt{\frac{\varepsilon_{\mathrm{Ag}}}{\varepsilon_{\mathrm{Ag}}+1}}\right] \tag{S1}$$

is the SPP mode index, and $\varepsilon_{\mathrm{Ag}}$ is the complex-dielectric permittivity of the template-stripped Ag-film at λ_0.

The total SPP round-trip loss in a Fabry-Perot resonator results from a combination of: (a) the absorption and scattering induced propagation loss of SPPs along the cavity floor, and (b) the absorption and scattering induced SPP reflection loss at each of the sidewalls. The propagation and reflection losses together limit the highest quality factor Q and Finesse $\mathcal{F}$ achievable using a Fabry-Perot cavity. For one round-trip propagation within a cavity of length l, the SPP power exponentially attenuates as $\exp(-2\alpha_s l)$, where $\alpha_s = 1/L_x$ is the SPP propagation loss-coefficient (where L_x is plotted in fig. S2). Combining propagation loss with the SPP reflectance R at each sidewall (fig. S3), the overall round-trip SPP attenuation is

$$r^2 = R^2\exp(-2\alpha_s l) = \exp(-2\alpha_r l)$$

where α_r is the effective overall distributed-loss coefficient given by

$$\alpha_r = \alpha_s + \frac{1}{2l}\ln\frac{1}{\mathcal{R}^2}$$

The finesse $\mathcal{F}$ of the SPP Fabry-Perot resonator (*36*) is expressed as

$$\mathcal{F} = \frac{\pi \exp(-\alpha_r l/2)}{1 - \exp(-\alpha_r l)}$$

and the quality factor Q is expressed as

$$Q = \frac{\nu_0}{\delta\nu} = \frac{c/\lambda_0}{c\alpha_r/2\pi}$$

where $\delta\nu = c\alpha_r/2\pi$ is the FWHM linewidth of the resonance and c is the speed of light in vacuum. The Fabry-Perot resonators used in this study are fabricated using Ag for the metal surfaces of the cavity and targeted to operate at a nominal resonant wavelength λ_0 = 650 nm, corresponding to a SPP wavelength λ_{SPP} = 625 nm (calculated using equation S1). The quality factor Q and Finesse $\mathcal{F}$ values for possible cavity-lengths l, corresponding to an integer multiple of $\lambda_{\text{SPP}}/2$, that support a resonance at λ_0 = 650 nm are shown in fig. S4B and C, respectively. These results clearly depict the tradeoff between quality factor Q and Finesse $\mathcal{F}$ for increasing cavity length l, where Q ($\mathcal{F}$) increases (decreases) with increasing l. For simplicity, we define a cavity figure-of-merit $\Gamma = Q * \mathcal{F}$ (fig. S4D) that exhibits a maximum value (Γ = 6750), corresponding to a simultaneously high value of quality factor and Finesse, respectively Q = 375 and $\mathcal{F}$ = 24, for a cavity length l = 2.5 µm (m = 8).

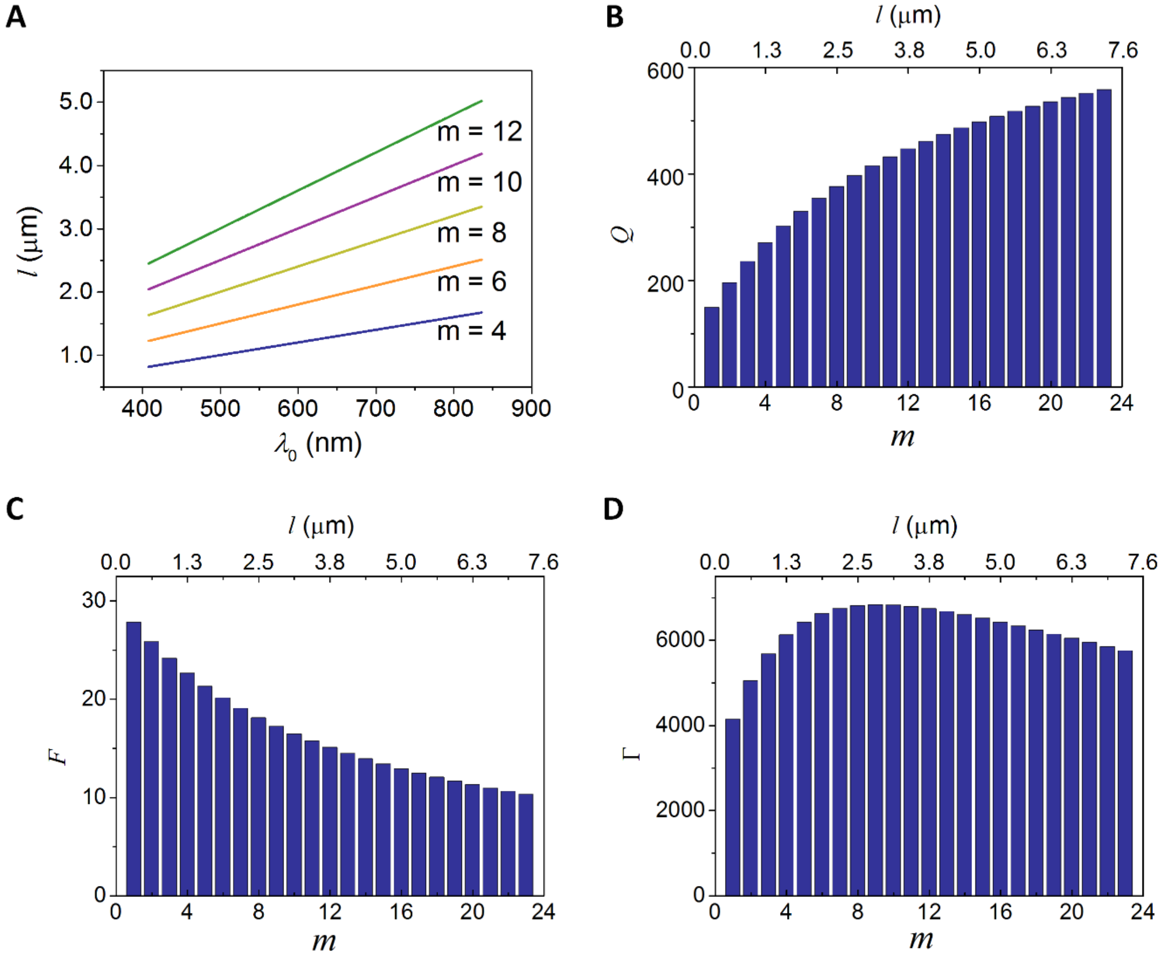

fig. S4. Design of an SPP resonator based on a lossy Fabry-Perot cavity model. (**A**) Cavity length corresponding to the trapping of an integer numbers (*m*) of SPP half wavelengths for free-space wavelength ranging from 400 nm to 850 nm. Variations in (**B**) Quality factor Q, (**C**) Finesse $\mathcal{F}$ and (**D**) Figure-of-merit Γ as a function of increasing cavity length l (or mode number m) for a cavity supporting a resonance at $\lambda_0 = 650$ nm vs. l (or m) for a pre-determined resonance wavelength. Simultaneously high values of Q, $\mathcal{F}$ and Γ are achieved for cavity length $l = 2.5$ µm ($m = 8$).

section S4. Optimization of the sampling-slit profile

The slit is engineered to couple to the field of the SPP standing wave with a minimum level of perturbation to the cavity resonance while still providing acceptable levels of transmission for observation. To achieve this, the slit is fabricated such that it does not intersect the plane of the cavity floor, but instead is recessed below the resonator floor by a distance δ (fig. S5A), establishing an intentionally weak evanescent link with the SPP mode trapped in the cavity. Moreover, the width of the slit at its closest point approaching to the cavity floor, σ, is simultaneously optimized for minimal perturbation. The dependence of Q on slit recess δ and end-width σ is explored using FDTD simulations, conservatively assuming a slit taper angle of 15° and a slit position laterally offset to the left of the center of the cavity by a distance $\zeta = 155$ nm. The simulations show that Q monotonically increases as a function of increasing recess δ and decreasing end-width σ. Consequently, the slit end-width is nominally set to $\sigma = 10$ nm, the smallest value anticipated to be achievable within the fabrication constraints of the present study. Simultaneously choosing a recess $\delta = 50$ nm yields a quality factor $Q = 350$, which is close to the maximum achievable value for a slit-free (unperturbed) cavity, $Q_0 = 375$. The simulated quality factor Q (fig. S5B) exhibits a periodic dependence on the lateral slit-position ζ, varying 180° out-of-phase with the surface magnetic field intensity, $|H_y|^2$, sampled at an equivalent position ζ along the floor of a slit-less, otherwise identical reference cavity illuminated under identical conditions. Q is observed to take on local maximum values at lateral slit-positions corresponding to the magnetic field nodes of the reference SPP standing wave, confirming minimum recessed-slit-induced scattering loss at such locations. The chosen slit offset of $\zeta = 155$ nm satisfies this condition.

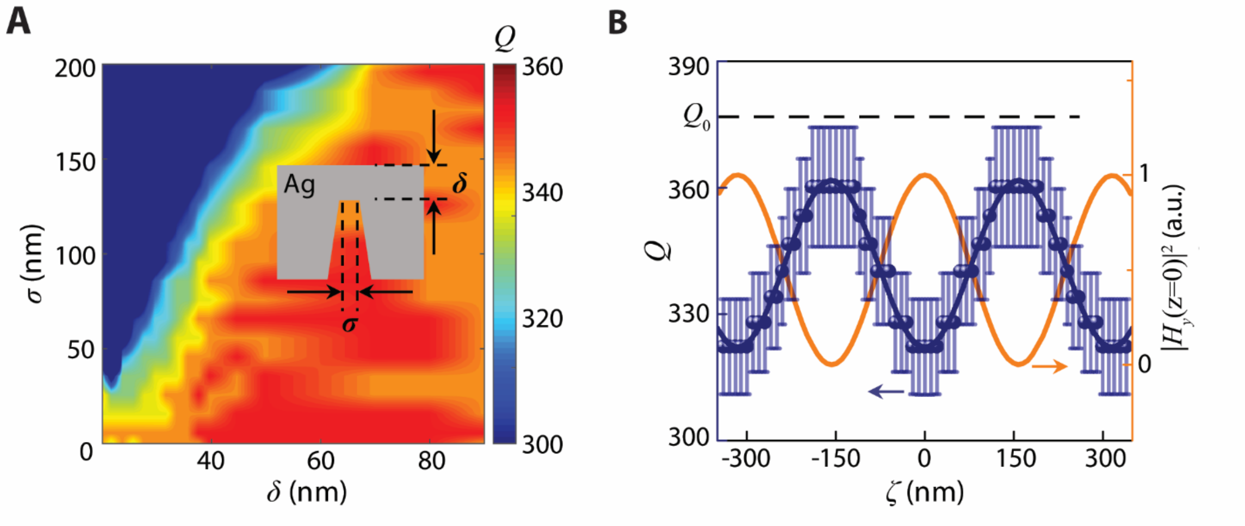

fig. S5. Optimization of the sampling-slit profile. (**A**) FDTD simulations of cavity quality factor *Q* vs. slit recess δ and end-width σ, assuming slit-sidewall taper angle = 15°, cavity length $l = 2.5$ µm, vertical mirror height $h = 2$ µm, free-space wavelength $\lambda_0 = 650$ nm. (**B**) Simulated *Q* (blue circles) along with sinusoidal fit (dashed blue line) vs. ζ, assuming cavity geometry of Fig. 1B**,** along with $\delta = 50$ nm and $\sigma = 10$ nm. Surface magnetic field intensity $|H_y|^2$ at each slit position ζ is displayed for reference (solid orange line). The uncertainties for the simulated *Q* are one standard deviation based on propagation of uncertainty from the Lorentzian curve-fitting of the resonance linewidths.

section S5. Fabrication process and optical characterization

Fabrication of the open-trench resonator for SPPs was performed using the template stripping method (*25*) with a pattern template consisting of a reusable, high-aspect-ratio Si mesa having a flat ultra-smooth top surface and near-vertical sidewalls.

As a first step in the fabrication of the Si mesa template, a layer of 50 nm-thick Si_3N_4 was deposited onto a silicon wafer via plasma-enhanced chemical vapor deposition. A 300-nm-thick spin-coated layer of poly-methyl methacrylate (PMMA) resist was then exposed with an inverse cavity pattern using electron-beam lithography at 100 keV, developed for 60 s in methyl isobutyl ketone (MIBK), and rinsed for 30 s in isopropyl alcohol (IPA). Room-temperature reactive ion etching and cryogenic (−110 °C) deep-silicon etching (*33*) were used consecutively to etch the

Si_3N_4 layer and Si, forming mesas of width $l \approx 2.5$ μm and height $h \approx 2.5$ μm. The wafer was then sequentially soaked in acetone and a nitride etchant (180 °C) to remove the PMMA resist and the Si_3N_4, respectively. The sidewall roughness of the Si mesa was effectively reduced by growing a 300-nm-thick layer of SiO_2 using an oxidation furnace (*34*), and subsequently removing the layer using hydrofluoric acid (HF). Si mesa was then exposed to a "piranha" etch solution to render it weakly adhesive to evaporated layers of metals such as Ag. Template fabrication was then finalized by patterning designed grating structures onto the Si mesa using low-current focused-ion-beam (FIB) milling.

As a first step in the formation of the open-trench resonator, Ag is angle evaporated onto the rotating Si template (at 70° with respect to the sample normal), to top-surface and sidewall thicknesses of ≈ 300 nm and ≈ 250 nm, respectively. A tapered-profile slit of subwavelength width is then patterned through the top-surface Ag-film, parallel to the mesa sidewalls, using low-current (1 pA), high resolution FIB milling, stopping short of the Ag-Si interface with a recess distance ≈ 50nm. The resulting slit width is ≈ 50 nm in the plane of the film and $\sigma \approx 10$ nm at its deepest point (as characterized by FIB cross-section analysis of a reference slit milled under identical conditions). Following application of optical-grade transparent epoxy, backing with a glass slide and thermal curing of the epoxy, mechanical stripping of the slide from the Si template then yields the final Ag open-trench structure, decorated with a subwavelength probing slit recessed below the cavity floor by distance $\delta \approx$ 50nm.

To transform the passive resonator into an active SPP lasing device, a thin layer of solid-state gain medium consisting of 3 mM dye (DCM) – doped PMMA is spin-coated onto the Ag floor of the trench, resulting in a nominal thickness at cavity center of ≈ 260 nm.

For passive cavity characterization, the samples were illuminated from the open side of the cavity with a halogen lamp (wavelength range: 450 nm to 850 nm). Light transmitted through the sampling slit was collected using 100× microscope objective ($NA = 0.75$) and directed to a triple-grating spectrometer connected to a cooled Si-CCD camera. Typical camera integration time was 30 s. A 150 grooves/mm grating was used to measure the broadband spectra and to find the resonance wavelength. A 600 grooves/mm grating that provides high spectral resolution was then used to characterize the corresponding resonance peak, from which the FWHM linewidth and the quality factor Q are determined. For plasmon laser characterization, a procedure similar to that used for passive characterization is followed, except that the optical source is replaced by a tunable nanosecond pulsed laser (λ_P = 480 nm, repetition rate = 10 Hz, pulse width ≈ 5 ns). A 514 nm long-pass filter is placed in front of the spectrometer entrance to block the residual pump. Typical camera integration time for these measurements was 10 s.

section S6. DCM material gain and spontaneous emission spectrum

The experimentally measured spontaneous emission spectrum of a 260 nm-thick PMMA:DCM deposited on a quartz substrate upon excitation with a nanosecond pulsed laser at λ_P = 480 nm is shown in fig. S6.

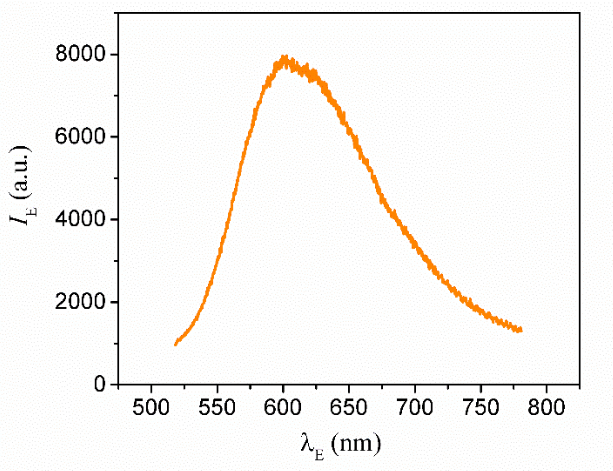

fig. S6. Spontaneous emission spectrum of PMMA:DCM. Experimentally measured spontaneous emission spectrum of a 260 nm-thick PMMA:DCM deposited on a quartz substrate upon excitation with a nanosecond pulsed laser at λ_P = 480 nm.

At the lasing wavelength λ_0 = 637 nm, for a cavity length $l \approx 2$ um, propagation loss $\alpha_s \approx 30\ \text{cm}^{-1}$, and sidewall reflectance $R \approx 0.95$, the calculated total SPP round-trip loss from Section III is determined to be $\alpha_r \approx 600\ \text{cm}^{-1}$. PMMA:DCM used here has been previously characterized as an optical gain medium and shown to provide a high gain efficiency K = 80 cm/MW (*27*). For the pumping intensity at threshold I_P = 10 MW/cm^2 used in our experiments, the calculated material gain is ≈ 800 cm^{-1}, which is larger than the calculated SPP round-trip loss – a prerequisite for lasing.

section S7. Fitting laser rate equation to experimental SPP emission

A simplified rate-equation model is adopted to study the dynamics of the photon–exciton interaction in the SPP laser cavity (*16*). The time-evolution of the exciton density n and emitted photon density s inside the cavity can be expressed using the set of coupled differential equations

$$\frac{dn}{dt} = \sigma p - An - \mathit{\Gamma} Asn$$

and

$$\frac{ds}{dt} = \beta An + \mathit{\Gamma} Asn - \gamma s$$

where σ is the exciton generation efficiency, p is the pump photon density, A^{-1} is the exciton lifetime inside the cavity, Γ is the gain-mode overlap factor, β is the spontaneous emission factor, and γ is the non-radiative photon lifetime in the cavity. The coupled rate equations are solved under the assumption that the SPP laser is pumped by a steady-state continuous-wave light, corresponding to a time-invariant pump photon density . The laser emission intensity, $I_E \propto s$, at steady-state is calculated for increasing pump power, $I_P \propto p$, and the pump-emission curve for various values of β are plotted on log-log and linear-linear scales (fig. S7A and B, respectively). The experimental estimate of β in Fig. 2D is achieved by fitting the solution of the rate equation to the experimentally measured pump-emission light-light curve.

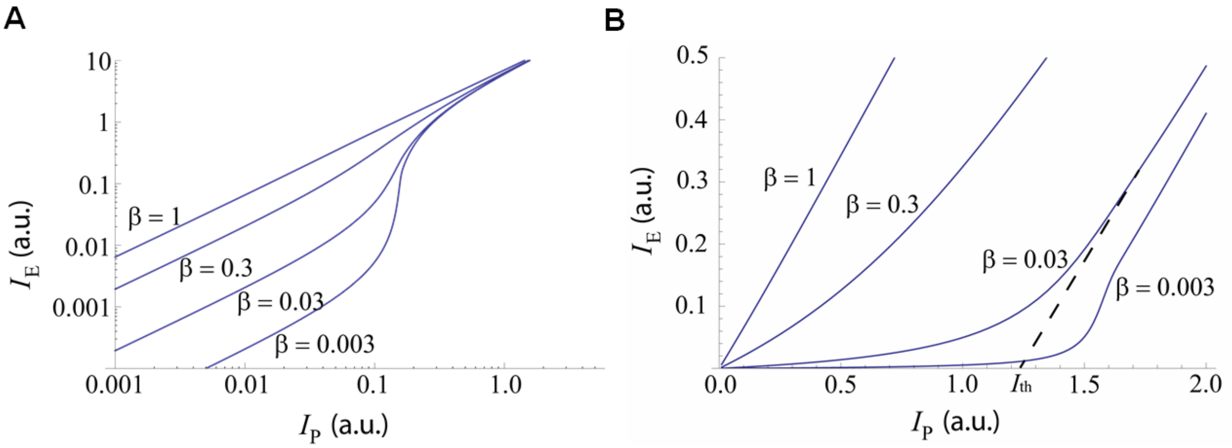

fig. S7. Laser emission as a function of varying the spontaneous emission factor. The emission intensity ($I_E \propto s$) as a function of the pump power ($I_P \propto p$), obtained by solving the laser rate equations for various values of spontaneous emission factor β, is plotted in (**A**) log-log scale showing the canonical "kink" behavior, and (**B**) linear-linear scale, showing the canonical lasing threshold behavior.

section S8. Numerical simulation of the SPP Fabry-Perot laser

FDTD simulations were used to demonstrate SPP lasing from a Fabry-Perot SPP resonator incorporating a layer of gain medium on the cavity floor and optically pumped from the cavity side. In the FDTD model, the cavity length, sidewall heights and slit-profile are set to the same values as those chosen for the optimized passive SPP resonator. The slit offset from cavity center, ζ', is however modified to coincide with a simulated node of the magnetic field of the SPP standing wave (see below). The simulated dye-layer thickness of 260 nm is chosen to match the dye-layer thickness at cavity center obtained upon spin coating of the experimental device (Fig. 2B). The gain medium is treated as a four-level system (*35*) with emission and absorption cross-sections exhibiting linewidth of $\approx$ 10 nm and centered at λ_E = 630 nm and λ_P = 480 nm, imbedded to a concentration N = 2×10^{18} cm^{-3} in host medium of relative dielectric constant 2.25 (mimicking PMMA). The cavity is pumped from its open side at normal incidence using a continuous-wave source at λ_P = 480 nm. The intensity of the transmitted light (I_E), out-coupled by the slit, and radiated on the substrate-side of the cavity is recorded at a distance of 500 nm below the slit as a function of increasing pump-power (I_P).

The FDTD modelled evolution of I_E vs. I_P, displaying a canonical "kink" shape on a log–log scale, is consistent with three distinct emission regimes characteristic of a standard laser as it transitions through threshold (fig. S8A), and closely matches in shape the experimentally measured transition through threshold for SPP lasing (Fig. 2C). The FDTD simulated magnetic field (at peak emission wavelength λ_E = 630 nm) resulting from pumping of the gain-medium-decorated cavity with an above-threshold pump-intensity $I_P = 2 \times 10^6$ W/cm^2 (at λ_P = 480 nm) is shown in fig. S8B. The magnetic field amplitude H_y is characterized by a laterally trapped SPP standing wave exhibiting twelve field-nodes (instead of the eight nodes observed in the case of the empty passive resonator, due to wave compression resulting from the background refractive index of the gain medium). Coincidence between the chosen slit position ζ' = 55 nm and a node of the magnetic field (the node closest to the cavity center) is achieved as designed.

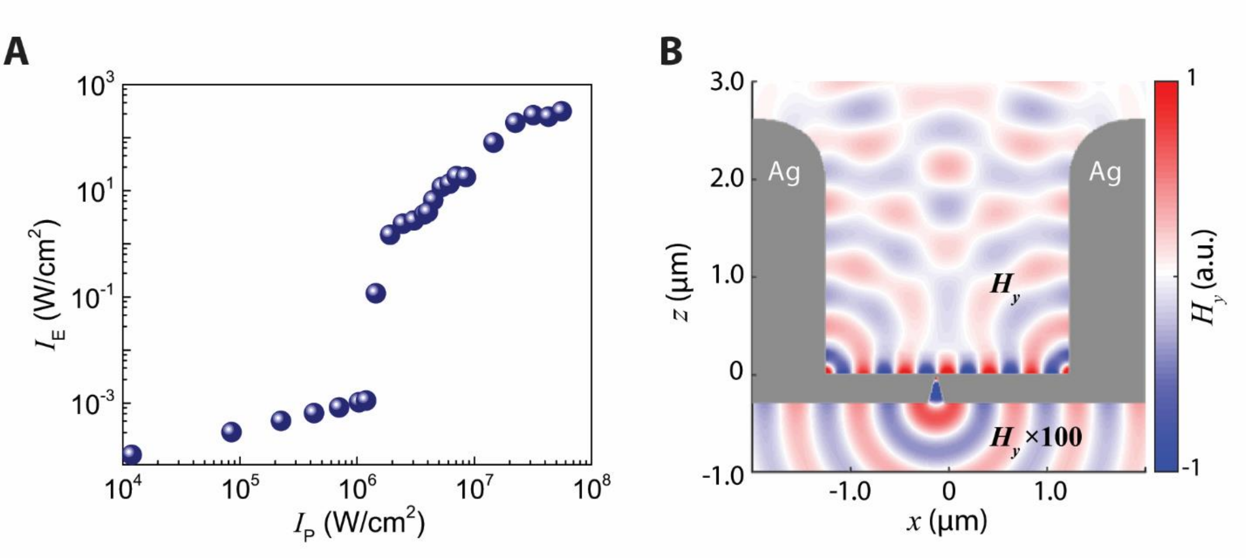

fig. S8. FDTD simulation of the SPP Fabry-Perot laser. (**A**) FDTD simulated log-scale light-light curve depicting the intensity of the slit out-coupled light emission, I_E (at λ_E = 630 nm), vs. pump intensity I_P (at λ_P = 480 nm). (**B**) FDTD simulated normalized H_y-field distribution at λ_E = 630 nm for pumping at λ_P = 480 nm with intensity $I_P = 2 \times 10^6$ W/cm^2. For ease of visualization H_y is multiplied by 100 in the plane below the cup-floor ($z < 0$).

section S9. Modal analysis of SPP modes in the presence of a thin dielectric layer

The dispersion curve of the SPP mode existing on a planar Ag film coated with a 260 nm-thick dielectric layer ($n = 1.45$) can be analytically calculated by solving the Maxwell equations (fig. S9). Within the visible frequency regime, the calculated effective refractive indices of the modes are larger than the refractive index of the dielectric layer, indicating that the modes are indeed SPP modes that evanescently decay from the surface. Based on these calculations, and also taking into account the frequency pulling effect (*37*), the estimated phase index and group index of the lasing SPP mode observed at peak wavelength $\lambda_E = 637$ nm are 1.54 and 1.96, respectively.

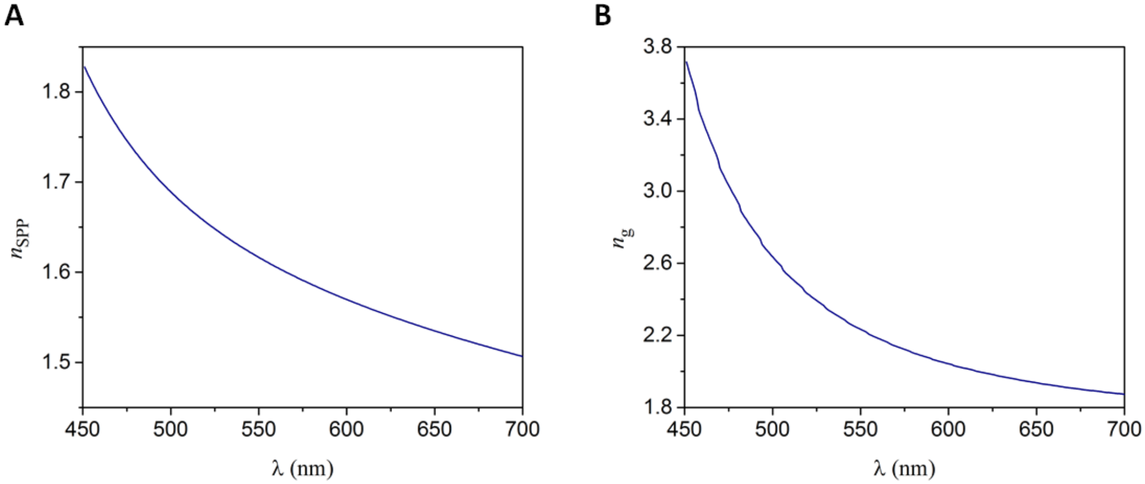

fig. S9. Dispersion of the lasing SPP mode. (**A**) Phase index and (**B**) group index of the SPP mode are analytically calculated by assuming a 260 nm–thick dielectric layer ($n = 1.45$) coated on top of a planar Ag film.

section S10. Morphology characterization of the tapered coupling grating

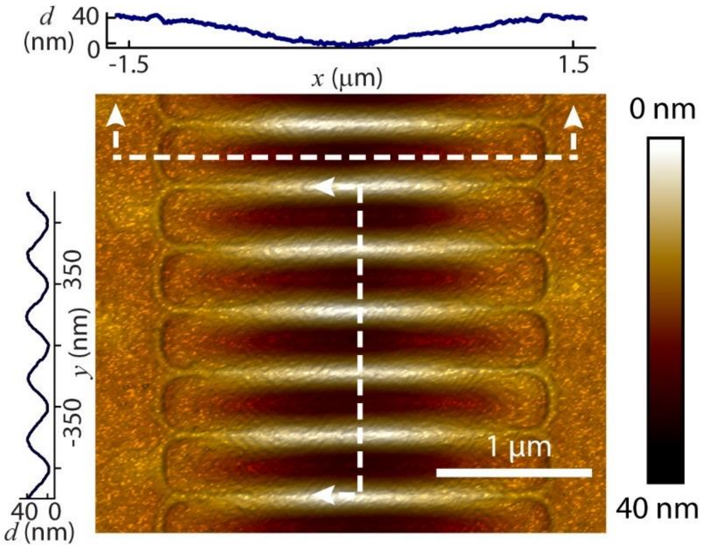

fig. S10. Morphology characterization of the inverse grating structure patterned on the Si mesa. AFM measurements of the Si mesa used for fabrication of grating-decorated SPP cavity. Horizontal cross-section (top panel) shows gently tapered profile modulated by one period of a cosine function with peak height *d* = 40 nm. Vertical cross-section (left panel) shows the sinusoidal grating profile with periodicity *p* = 350 nm. The morphology of the final template-stripped grating-decorated SPP cavity is directly inferred using this AFM measurement.

section S11. Optimization of the SPP-pumped SPP laser

The threshold of the SPP-pumped SPP laser is also closely related to the periodicity and the peak height of the low-profile grating. The lowest threshold is achieved with *p* = 350 nm (fig. S11A), which matches the maximum pump SPP coupling efficiency at λ_P = 480 nm for a 260 nm-thick dielectric layer on top of the grating. Similarly, considering the trading-off between the SPP-coupling efficiency and the scattering of the SPP emission mode, the lowest threshold is achieved with *d* = 40 nm (fig. S11B). Note that lasing behavior was not observed for the device with *d* = 80 nm wherein the laser gain was not able to compensate for the additional loss incurred on the SPP emission mode due to grating-induced scattering.

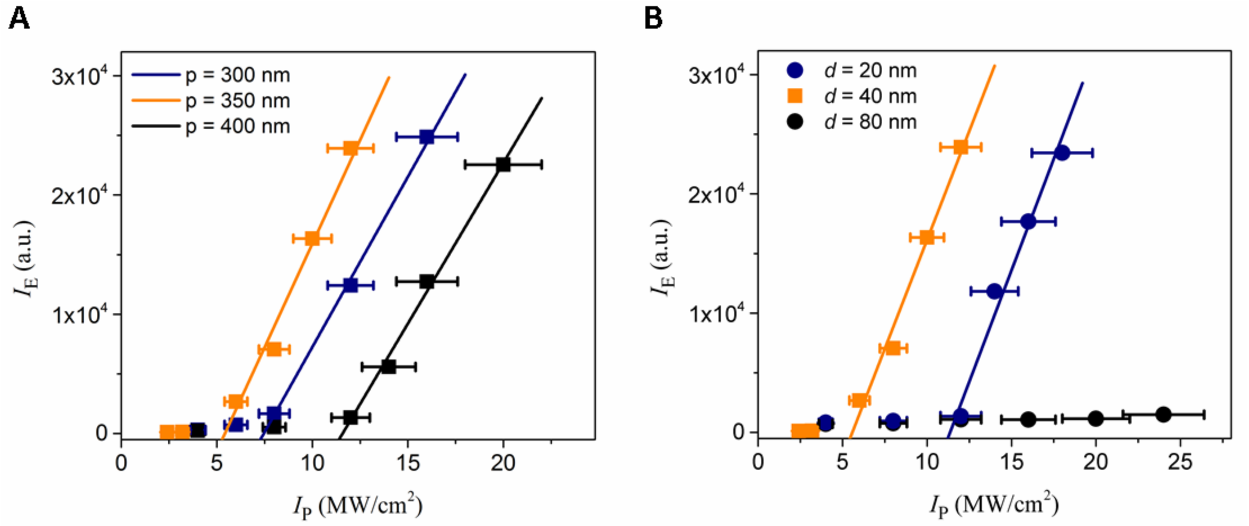

fig. S11. Grating optimization of the SPP-pumped SPP laser. Lasing turn-on characteristic of the SPP-pumped SPP lasers having (**A**) different grating periodicities p = 300 nm, 350 nm and 400 nm (for the chosen nominal peak height d = 40 nm) and (**B**) different peak heights d = 20 nm, 40 nm and 80 nm (for the chosen nominal grating periodicity p = 350 nm).

section S12. Simulation of grating-coupled pump SPPs

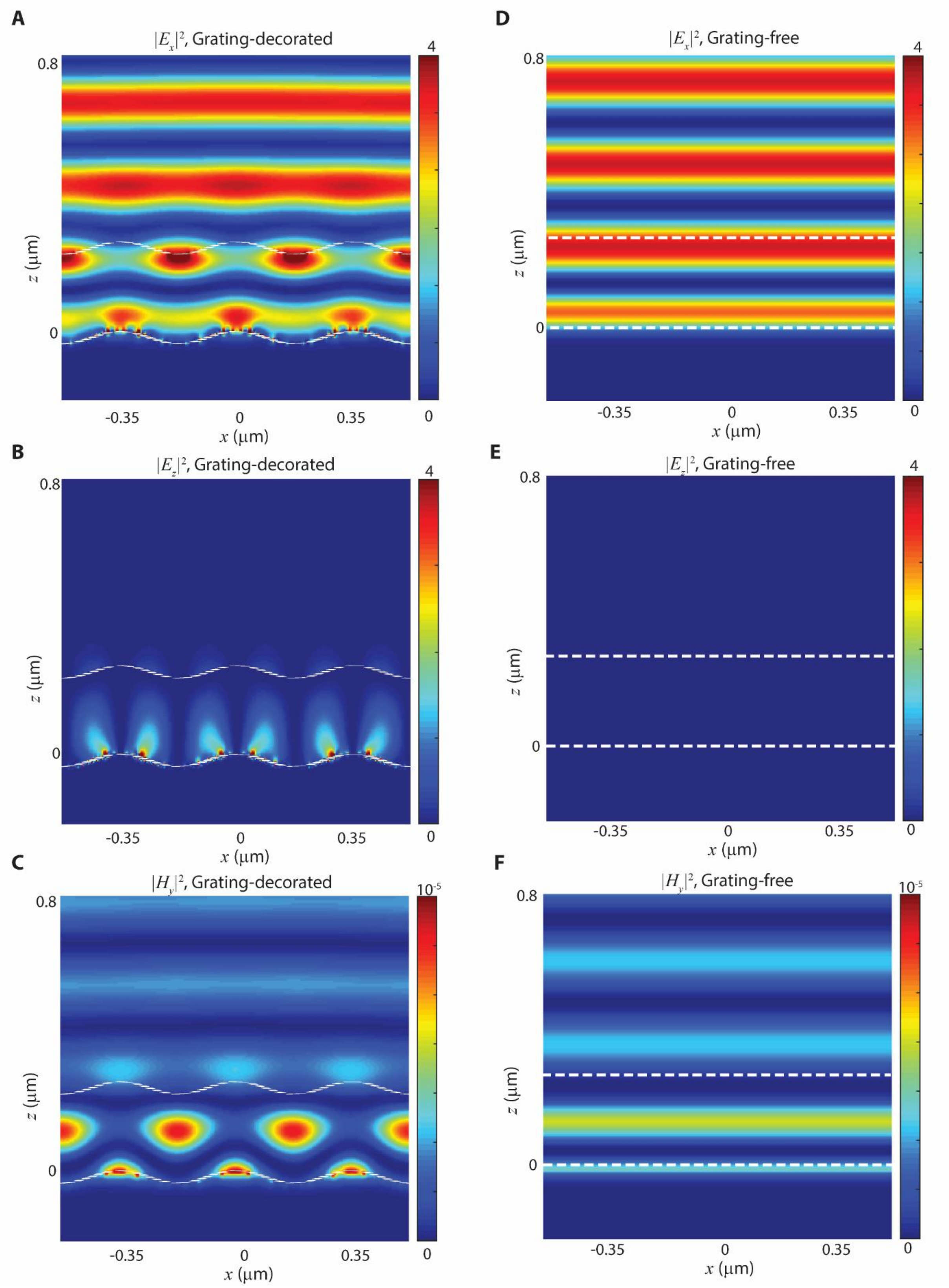

fig. S12. Simulated steady-state intensity profiles for grating-decorated and grating-free Ag surfaces coated with a 260-nm-thick four-level gain medium. (**A** to **C**) steady-state intensity profiles $|E_x|^2$, $|E_z|^2$, and $|H_y|^2$ for a normal-incidence pump beam at λ_P = 480 nm for a grating-decorated Ag surface with periodicity p = 350 nm. (**D** to **F**) Corresponding steady-state intensity profiles $|E_x|^2$, $|E_z|^2$, and $|H_y|^2$ for a grating-free surface illuminated under identical conditions. The presence of an $|E_z|$ field component above the corrugated metal surface (B), along with the presence of a non-zero electrical field component (B, C) at the interface between the metal and the dielectric confirm generation of pump-SPPs in the case of the grating–decorated Ag surface. In contrast, the pump field pattern above the grating-free metal surface displays a complete absence of field-component $|E_z|$ (E) along with a minimum in component $|E_x|$ at the surface (D) indicating a SPP-free vertical standing-wave above the reflective surface. Dashed white lines indicate the grating surface and boundaries of the four-level gain medium. The power absorbed by the gain medium is greater by a factor of 1.5 in the case of a grating-decorated Ag surface in comparison to that of the reference grating-free Ag surface.